Progress in Oceanography 79 (2008) 167–176

Contents lists available at ScienceDirect

Progress in Oceanography

journal homepage: www.elsevier.com/locate/pocean

The seasonal cycle of surface chlorophyll in the Peruvian upwelling system: A modelling study

V. Echevin [a,*], O. Aumont [a,c], J. Ledesma [b], G. Flores [b]

[a] LOCEAN/IRD/IPSL, Laboratoire d'Océanographie et de Climatologie: Expérimentation et Approches Numériques, IRD/UPMC/IPSL, Paris, France
[b] IMARPE, Esquina de Gamarra y General Valle S/N Chucuito Callao, Peru
[c] Centre IRD de Bretagne, Plouzané, France

ARTICLE INFO

Article history:
Accepted 14 October 2008
Available online 21 October 2008

ABSTRACT

The seasonal variability of surface chlorophyll in the northern Humboldt Current System is studied using satellite data, *in situ* observations and model simulations. The data show that surface chlorophyll concentration is highest in austral summer and decreases during austral winter, in phase opposition with coastal upwelling intensity. A regional model coupling ocean dynamics and biogeochemical cycles is used to investigate the processes which control this apparently paradoxical seasonal cycle. Model results suggest that the seasonal variability of the mixed layer depth is the main controlling factor of the seasonality. In winter, the mixed layer deepening reduces the surface chlorophyll accumulation because of a dilution effect and light limitation. In summer, biomass concentrates near the surface in the shallow mixed layer and nitrate limitation occurs, resulting in a biomass decrease in the middle of summer. Intense blooms occur during the spring restratification period, when winter light limitation relaxes, and during the fall destratification period, when the surface layer is supplied with new nutrients. Model sensitivity experiments show that the seasonal variations in insolation and surface temperature have little impact on the surface chlorophyll variability.

1. Introduction

The Peruvian upwelling system (the nearshore 250 km of the Humboldt Current; hereafter PUS) is one of the most intense upwelling systems in the world ocean. Relatively weak, seasonally varying, upwelling-favorable winds drive an offshore Ekman transport and an upward flux of cold, nutrient-rich waters along the coast. The presence of nutrient-rich waters and high insolation at this low latitude generates a year-long but fluctuating phytoplankton bloom which sustains a very rich ecosystem with high stocks of pelagic fish (FAO, 1999). The subsurface waters off Peru have very low oxygen concentrations (Minas et al., 1990), due to low ventilation (Wyrtki, 1962) and to oxygen consumption by the organisms remineralizing the abundant organic matter sinking from the surface (Paulmier et al., 2006). These processes lead to the formation of one of the most intense oxygen minimum zones of the world ocean, whose impact on the surface productivity and on the overlying pelagic ecosystem remains an open question.

The PUS is influenced by the variability of equatorial origin at intraseasonal (Bonhomme et al., 2007) and interannual time scales (Carr et al., 2002). Equatorial variability can propagate along the coast as far south as 40°S (Ulloa et al., 2001) in the form of coastally trapped waves. The upwelling system is also subject to decadal climate variability as shown by the very long time series of ecosystem indices (Chavez et al., 2003). Although the intense nearshore biological activity is related to the wind-driven coastal upwelling, the response of the ecosystem to the wind varies significantly depending on the time scales. Indeed, the seasonal fluctuations of surface productivity, as observed by satellite and *in situ* surface chlorophyll measurements (Chavez et al., 1995, Thomas et al., 2001; Pennington et al., 2006, hereafter PEN06) and of wind intensity, are in opposition. Surface chlorophyll decreases in austral winter, the period during which coastal upwelling and nutrient supply from the subsurface is supposed to be strongest (Calienes et al., 1985). The coupled physical-biogeochemical processes governing this counter-intuitive variability have not been fully investigated, nor their relative impacts quantified. Calienes et al. (1985) suggested that the mixed layer depth increase in winter could reduce surface chlorophyll through light limitation of phytoplankton growth. Guillen and Calienes (1981) also invoke the potential role of low solar insolation in winter. However, other processes may have an impact, such as the seasonal variations of surface macro and micro-nutrient concentrations driven by the upwelling variability, or the surface temperature variations. In the present work, we investigate these processes using ocean color satellite data, *in situ* observations and model simulations. This approach allows evaluation of the relative role of the processes involved. In the following section (Section 2), the data, model and methodology are described. The results are presented in Section 3, and are discussed

* Corresponding author.
E-mail address: vincent.echevin@locean-ipsl.upmc.fr (V. Echevin).

0079-6611/$ - see front matter © 2008 Elsevier Ltd. All rights reserved.
doi:10.1016/j.pocean.2008.10.026

in Section 4. Conclusions and perspectives are outlined in Section 5.

2. Materials and methods

Surface chlorophyll concentrations were studied using two different data sets. First, we used *in situ* chlorophyll observations collected by IMARPE (Instituto del Mar del Peru) during 1992–2004 (Fig. 1a). A complete description of the *in situ* data processing and quality control is provided in Appendix A gridded product was constructed as follows: the data for each month of the 1992–2004 period were first binned in a 0.5° × 0.5° grid. Extreme values were filtered out (in log scale) by removing values higher than twice the standard deviation in each spatial bin. The data were then averaged, and transformed into real, i.e. non-log, values, for each month. Data collected during the El Nino years in the 1997–1998 period were included.

Second, we used the SeaWiFS chlorophyll product (version 4 chlorophyll algorithm) for October 1997–December 2004 (Fig. 1b). The data (8-day chlorophyll-*a* composites) were rebinned from the original 0.0879° × 0.0879° grid in a low resolution (0.5° × 0.5°) grid to reduce the noise, the effects of clouds, and the impact of the very high chlorophyll concentrations very close to the shore, which may be unrealistic. The monthly climatology was constructed by removing extreme values (higher than twice the standard deviation in log scale), and averaging log-scale data for each month and for each pixel.

The third data set consists of *in situ* nutrient (nitrate, phosphate, silicate) concentrations collected by IMARPE during 1992–2004. As with the *in situ* chlorophyll data, a gridded product was constructed by binning and averaging the data in a 0.5° × 0.5° grid, after filtering out the extreme values (higher than twice the standard deviation) in each bin. The protocol for processing the nutrient data is also described in the Appendix.

Last, outputs from a numerical model were used to study the different processes governing surface chlorophyll in the upwelling system. To this end, the Regional Ocean Modelling System circulation model (ROMS, Shchepetkin and McWilliams, 2005) and the biogeochemical model (PISCES, Aumont et al., 2003; Aumont and Bopp, 2006) have been coupled:

- The Regional Ocean Modelling System (ROMS) is a free surface, sigma coordinate, primitive equation model. In the present study, the horizontal resolution is 1/6°. ROMS has 30 levels in the vertical, with an increase of resolution near the surface. Because of the use of sigma coordinates, the resolution in the vertical varies depending on the water column depth. The surface layer thickness ranges from a minimum of 10 cm in a 50-m deep nearshore water column, to 6 m in a 4000-m deep water column. Similarly, the bottom layer thickness ranges from 9 m to 900 m. The model configuration used here is very similar to that in Penven et al. (2005), but with a coarser horizontal resolution (1/9° in Penven et al., 2005). For a more complete description of the dynamical model configuration and numerical schemes, the reader is referred to Penven et al. (2005) and to Shchepetkin and McWilliams (2005) respectively.
- PISCES (Pelagic Interaction Scheme for Carbon and Ecosystem Studies) is a biogeochemical model derived from the Hamburg Model of Carbon Cycle, version 5 HAMOCC5 (Aumont et al., 2003). PISCES simulates biological productivity and the biogeochemical cycles of carbon and of the main nutrients (Phosphate, Nitrate, Ammonium, Silicate and Iron). It assumes that phytoplankton growth is directly limited by the external availability in nutrients, and includes two phytoplankton size classes (nanophytoplankton and diatoms), two zooplankton size classes (microzooplankton and mesozooplankton) and two detritus size classes. Diatoms differ from nanophytoplankton by their need for Si, by higher requirements for Fe (Sunda and Huntsman, 1997), and by higher half-saturation constants because of their larger size. PISCES has previously been coupled with the OPA (Madec et al., 1998) ocean general circulation model at coarse spatial resolution (2° and 1/2°) and used in global (Aumont et al., 2003; Aumont and Bopp, 2006) and basin-scale studies (Gorgues et al., 2005).

Here PISCES is coupled to ROMS to address regional and coastal issues. The technical procedure for coupling the ecosystem and dynamical model components follows that of Gruber et al. (2006), who coupled ROMS with a slightly simpler ecological–biogeochemical model than PISCES. Readers are referred to the papers by Aumont et al. (2003) and Aumont and Bopp (2006) for further details on the PISCES model equations.

A climatological simulation has been performed using monthly mean values at the model open boundaries. The dynamical variables (temperature, salinity, velocities) at the boundaries are specified using climatological values of ORCA 0.5° OGCM during 1992–2000. A time series covering the entire 1992–2005 period was not available, but the 1992–2000 series appears sufficiently

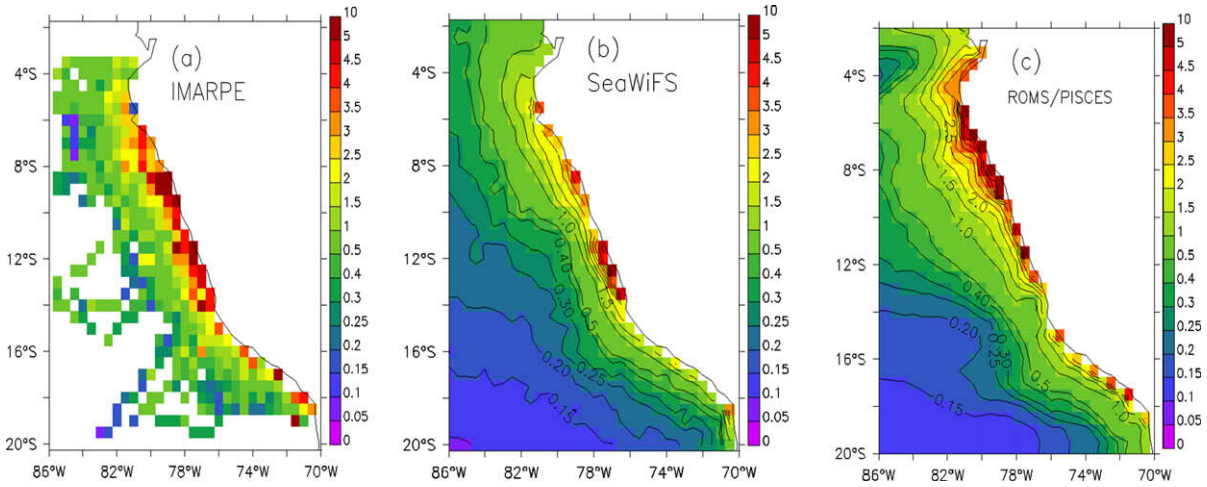

Fig. 1. Average surface chlorophyll (in mgChl/m^3): (a) IMARPE in situ data (1992–2004); (b) SeaWIFs data over the years 1997–2004; (c) ROMS/PISCES model (interpolated onto a 0.5° × 0.5° grid).

long to filter the interannual variability and to represent the large scale dynamical climatological circulation and water mass characteristics. The biogeochemical variables (nutrients and oxygen) are specified using nitrate, phosphate, silicate and oxygen monthly values from the World Ocean Atlas 2001 (Conkright et al., 2002). As boundary estimates of Fe were not available from data climatologies, they were extracted from a climatology of the global, interannual, coupled ORCA-PISCES simulation at 2° resolution, as was performed by Aumont and Bopp (2006).

The surface atmospheric forcing for ROMS consists of a Quikscat wind stress monthly climatology calculated over 1999–2003 as in Penven et al. (2005). This time period was chosen instead of 1992–2000, as the Quikscat product is of better quality than the ERS data because of its higher spatial resolution near the Peruvian coasts (Croquette et al., 2007). Heat fluxes, SST and SSS from the COADS monthly climatology (Da Silva et al., 1994) were also used following Penven et al. (2005). The surface forcing for PISCES includes Fe atmospheric deposition, which was calculated from the model results of Tegen and Fung (1995), assuming constant values for the iron content and the solubility.

ROMS/PISCES was run for a period of eight years, and reached a statistical quasi-equilibrium after a spin-up phase of five years. The final three years of simulation (years 6–8) are used to construct a monthly climatology.

3. Results

3.1. Spatial pattern of surface chlorophyll – in situ, satellite and ROMS/PISCES

The surface chlorophyll maps, averaged over a period of several years, display spatial patterns typical of coastal upwelling (Fig. 1). Chlorophyll concentrations are maximum nearshore (5–10 mgChl/m^3) and decrease gradually offshore, reaching ~0.5–1.5 mgChl/m^3 at 200–300 km from the coast. The richest nearshore areas are between 6°S and 15°S, with local chlorophyll maxima near 9°S, 12°S and 14°S in the *in situ* map (Fig. 1a), and near 12–14°S in the satellite data (Fig. 1b). Along the coast north of 6°S, surface chlorophyll values are low in both *in situ* and satellite observations, whereas south of 15°S, the satellite chlorophyll is lower than the *in situ* data. The cross-shore gradient of *in situ* chlorophyll seems rather independent of the latitude, whereas chlorophyll-rich waters observed by satellite are closer to the coast.

These time-average values of *in situ* (Fig. 1a) and satellite data (Fig. 1b) are generally consistent with each other, and in agreement with previous studies (Chavez, 1995). The highly productive zone (4–10 mgChl/m^3) is narrower in the satellite data when compared with the *in situ* observations. However, it is well known that the SeaWiFS inverse algorithm used to calculate surface chlorophyll from radiances tends to underestimate the high concentrations in coastal zones (Hooker and McClain, 2000), which may account for part of this bias. Moreover, this nearshore underestimate of chlorophyll by SeaWIFS may be exacerbated by the frequent nearshore cloud coverage, especially in winter, which could prevent the sampling of some of the intense surface blooms.

ROMS/PISCES surface chlorophyll values are shown in Fig. 1c, where the model output has been interpolated onto the same 0.5° by 0.5° horizontal grid as the observations. The modelled chlorophyll concentrations agree reasonably well with the observations in magnitude. Maximum values of ~5–10 mgChl/m^3 occur within 25–50 km of the coast. Maximum nearshore values are encountered from 5°S to 9°S. The chlorophyll cross-shore gradient is rather similar in the observations and in the model as shown by the cross-shore slope of chlorophyll (Fig. 2) The offshore chlorophyll values are close in the satellite data and *in situ* observations. Modelled large phytoplankton cells (diatoms) are mostly responsible for the biomass increase towards the coast (Fig. 2). This group is known to become dominant in nearshore Peruvian waters (Iriartre and Gonzalez, 2004; DiTullio et al., 2005). Thus the model seems to represent the shift between the nearshore and offshore plankton communities. This contrasts with other modelling studies based on more simple ecosystem models, which are not able to represent this cross-shore transition (Gruber et al., 2006).

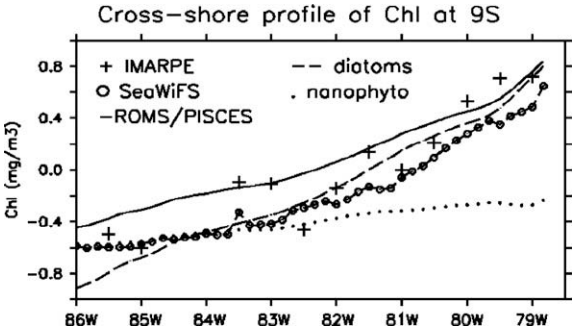

Fig. 2. Cross-shore profile of surface chlorophyll (in mgChl/m^3, in log scale) at 9°S for SeaWiFS (circles) data, IMARPE in situ observations (crosses), and ROMS/PISCES model. The full line corresponds to the model total chlorophyll, the dashed line to the chlorophyll content in diatoms, the dotted line to the chlorophyll content in the nanophytoplankton, respectively.

Some model biases appear in Fig. 1c. North of 6°S, the rather high nearshore chlorophyll (~3–4 mgChl/m^3) may be caused by excessive coastal upwelling in the model. In contrast, south of 10°S, modelled nearshore chlorophyll is slightly lower than the observations and the productive zone is quite narrow (note the tight isolines near 14°S in Fig. 1c). The nearshore modelled chlorophyll remains rather low as far south as 15°S, despite the strong upwelling center near Paracas (Strub et al., 1998).

3.2. Seasonal variability of surface chlorophyll

3.2.1. Average seasonal cycle

We first study the surface chlorophyll seasonal cycle by averaging all the available data over a coastal box, which roughly defines the boundaries of the PCUbiogeochemical province. In a recent paper, PEN06 defined such a province as a coastal zone of 250 km cross-shore width, ranging from 4°S to 15°S. They computed a seasonal cycle by averaging all the surface chlorophyll *in situ* data available in this box, for each month of the year. The same calculation was repeated with SeaWiFS data during the September 1997–May 2005 period. We proceeded identically by averaging the IMARPE, SeaWiFS and model data over a the same domain. All the *in situ* data collected during 1992–2004 were used in order to compile a sufficient amount of observations. Restricting our data set to the same period studied by PEN06 would have reduced the accuracy of the calculated seasonal cycle (see Table 1).

Results from PEN06 and our study are presented in Fig. 3. The two SeaWiFS time series are very consistent: both display a single chlorophyll maximum in late austral summer and a minimum in austral winter. We verified that the seasonality portrayed in Fig. 3b is not modified when the year 2005 (used in PEN06) is included in our SeaWiFS time series (not shown).

The model seasonal cycle is also consistent. data (Fig. 3b). The modelled chlorophyll is high in austral summer – with a slight decrease in February – and low in austral winter. Note that the model values are significantly higher than the SeaWiFS values, closer to the IMARPE *in situ* data.

Let us now examine the differences in seasonal cycle. The two *in situ* time series display notable differences. The PEN06 *in situ* time series (Fig. 3a) displays two maxima – in early (November) and late austral summer (April), and a minimum in winter

Table 1
Monthly-mean IMARPE *in situ* chlorophyll (in mgChl/m^3) in a 200 km-wide coastal box between 6°S and 15°S during the 1992–2004 period.

	1992	1993	1994	1995	1996	1997	1998	1999	2000	2001	2002	2003	2004
Chjan	2.0(3)	1.7(1)	4.9(1)	1.8(17)	2.9(4)		1.1(1)	1.0(1)	2.4(14)	3.8(1)	1.9(1)	3.4(7)	3.6(12)
Chlfeb	3.1(66)	6.0(47)	2.2(1)	2.3(13)	1.5(7)	2.2(4)	1.1(1)	1.6(20)	2.2(61)	2.5(1)	6.1(4)	6.3(4)	3.8(28)
Chlmar		3.7(20)		3.9(66)	3.4(61)		1.3(3)	1.3(45)	5.4(11)	3.1(42)	4.9(15)		
Chlapr	1.0(2)	3.4(1)	2.1(1)	1.7(3)	7.9(3)	5.0(1)	0.9(13)	2.8(1)	0.66(2)	6.4(3)	3.8(4)	5.8(5)	8.3(4)
Chlmay	1.5(4)	5.6(1)	5.3(1)	1.0(28)	5.4(16)	3.1(1)	0.9(21)	1.4(21)	2.7(18)	4.9(1)	2.1(1)	1.8(15)	2.4(1)
Chljun	1.8(2)	0.5(1)	2.8(1)	0.2(17)	3.6(13)	1.2(11)	1.9(1)	3.5(1)	4.3(3)	7.5(4)	5.0(4)	2.0(6)	2.4(4)
Chljul	1.5(7)	2.6(1)	1.7(1)	0.1(4)	5.9(1)	4.7(14)	1.0(1)	2.4(1)	2.2(1)	0.9(1)	2.4(1)	2.6(4)	1.4(1)
Chlaug	3.1(5)	10.2(1)	2.1(48)	2.3(42)	2.6(44)	1.0(1)	0.9(16)	2.1(1)	3.4(13)	1.4(4)	2.2(77)	2.3(28)	1.6(46)
Chlsep		5.8(1)	3.7(22)	7.8(30)	2.9(49)	1.6(32)	0.8(56)	1.7(21)	3.6(50)	8.6(1)		1.9(23)	3.1(12)
Chloct	7.3(1)	2.3(1)	3.9(4)	1.0(1)	8.3(1)	1.7(16)		1.2(1)	2.9(4)	1.6(3)	1.1(22)	2.3(13)	6.5(11)
Chlnov	1.9(3)		1.3(8)	5.4(32)	1.9(28)		3.2(1)	3.3(25)	5.3(1)	8.7(1)	3.4(3)	2.1(49)	7.0(23)
Chldec		3.5(21)	2.2(16)	6.6(20)	2.8(60)	1.1(1)		4.1(46)	1.1(3)	7.6(4)	3.0(8)	2.8(9)	3.7(47)

The value in brackets indicates the number of 0.5° × 0.5° grid points averaged to compute the monthly mean. When only one grid point is available, the single data point from the Callao (78 °W, 12°S) time series was used.

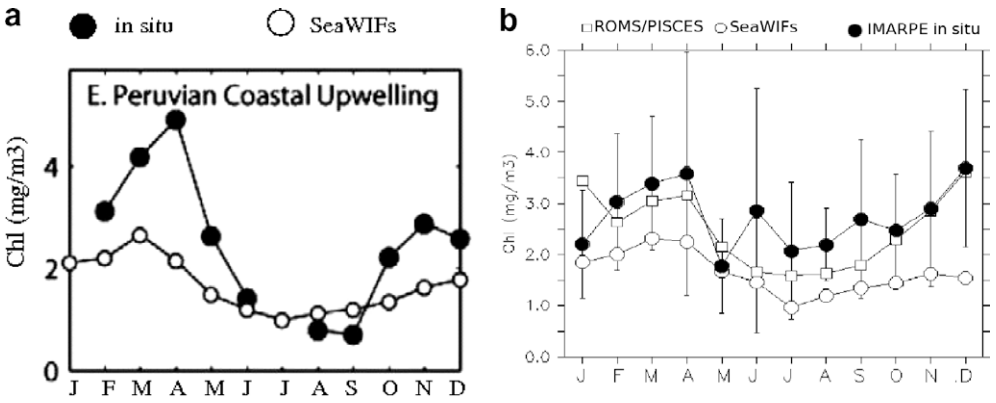

Fig. 3. Seasonal cycle of the surface chlorophyll concentration (in mgChl/m^3) averaged over a coastal box of 250 km zonal width between 4°S and 15°S: (a) in situ (black circles) and SeaWIFs (white circles) data during 1997–2005 (courtesy of Pennington et al., 2006); (b) ROMS/PISCES model (white squares), SeaWIFs (white circles), in situ IMARPE data (black circles), during 1992–2004. Vertical bars correspond to the interannual variability of the in situ data set.

(Fig. 3a). In contrast, the IMARPE time series (Fig. 3b) displays high (but lower than PEN06) values in austral summer, and low values in January, May and in austral winter (July–August). In contrast to PEN06, the IMARPE surface chlorophyll in austral winter remains relatively high (Fig. 3b). These differences during austral winter could be related to differences in data sampling. Indeed, the vertical bars plotted in Fig. 3b indicate the variance of the monthly mean values in the 1992–2004 period, thus the high interannual variability in monthly means. Months with poor sampling (i.e. with less than two observations in the coastal box, see Table 1) were not taken into account in the statistics. Overall, the *in situ* time series are in good agreement with one another, except for the relatively higher values in austral winter in the IMARPE data set.

The model average seasonal cycle is relatively similar to the observed ones. Even though the model values are overestimated in January, the surface phytoplanktonic biomass displays the same seasonal tendency as the observations: chlorophyll is high in austral summer, and reaches a minimum in austral winter as the wind-driven upwelling is supposed to strengthen (Bakun and Nelson, 1991).

3.2.2. Alongshore variations of the seasonal cycle

Alongshore variations of the surface chlorophyll seasonal cycle are portrayed in Fig. 4. The SeaWiFS and model chlorophyll values within a 200 km-wide coastal band were binned for each month and each latitude. The IMARPE data set was not comprehensive enough to study alongshore variations because of low sampling during some months (e.g. April, see Table 1).

Let us first describe the alongshore variability observed by SeaWiFS (Fig. 4a). Several patterns can be emphasized. First, the phase of the seasonal cycle depends little on latitude. From 7°S to 14°S, high values are encountered in late austral spring and early summer (October–November–December). In austral spring (October), chlorophyll is high (greater than 1.5 mgChlm^{-3}) in three narrow latitude bands (6–7°S, 8–9°S and 11–14°S, Fig. 4a), and decreases near 10–11°S. Two isolated points near 10°S and 12°S in August (Fig. 4a) suggest that high chlorophyll values may occur in austral winter as well. However, this signal is not very well sampled because of the higher cloud coverage during this season.

The model alongshore variations of modelled chlorophyll agree relatively well with the satellite data in the north of Peru (Fig. 4b). The modelled values are high during austral spring and summer with a slight decrease in February. Maximum concentrations are reached during late austral spring near 7°S in the model, and during late summer in the observations. The maximum modelled values (~6–7 mgChl/m^3) are higher than the maximum SeaWiFS values (~4 mgChl/m^3). The lowest chlorophyll values are reached during the winter months (July–August–September). Between 10.5°S and 11°S, the model's seasonal variability decreases, consistently with SeaWiFS data. South of 13°S, the model is not realistic, as shown by the low chlorophyll concentration (less than 1.5 mgChl/m^3) all year long.

3.3. Seasonal variability of the chlorophyll content in the euphotic layer

As noted previously, the evolution of surface chlorophyll does not seem to be controlled by lack of nutrients in the surface layer, which increases in austral winter due to the more upwelling-favorable winds during this season (Fig. 5a). The question we now ad-

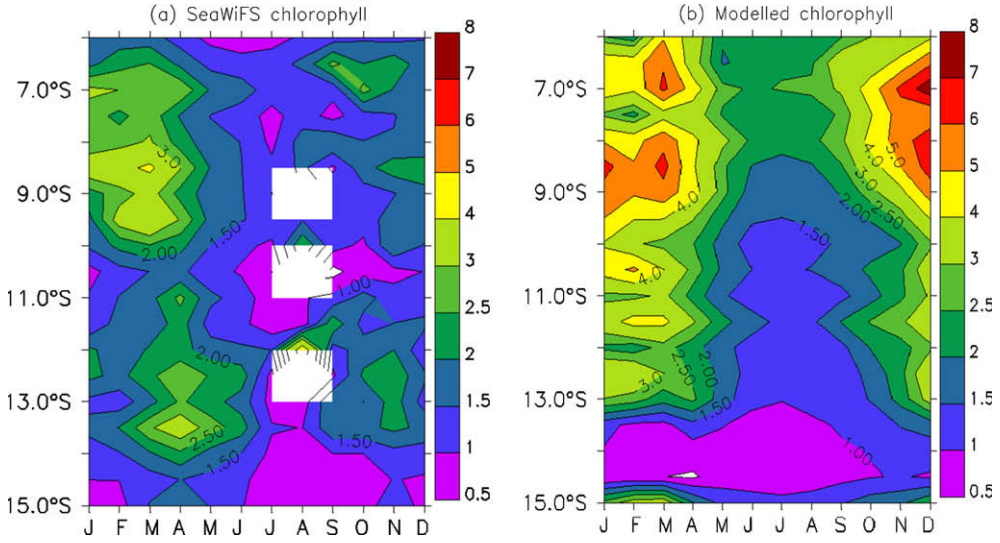

Fig. 4. Latitude-time variations of the surface chlorophyll concentration (in mgChl/m^3) in a 200 km-wide coastal band: (a) SeaWIFs; (b) ROMS/PISCES model. Contour values are identical to the color scales.

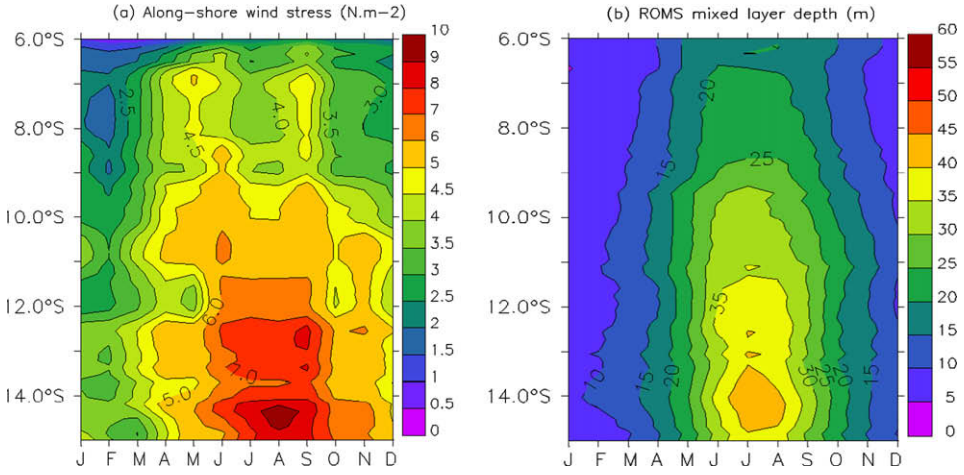

Fig. 5. Time–latitude variations: (a) alongshore wind stress (in N m^{-2}) from a 1999–2003 Quikscat climatology; (b) ROMS/PISCES mixed layer depth (in m). Both variables are averaged in a 200 km-wide coastal band.

dress is the following: what is the impact of vertical mixing due to the winter trade winds increase? Could this process drive a decrease in surface chlorophyll concentrations by distributing phytoplankton over a thicker mixed layer? Fig. 5b displays the evolution in time of the model mixed layer depth (hereafter MLD), defined as the depth where the local Richardson number reaches the critical value of 0.3 (Large et al., 1994). MLD values increase significantly during austral winter and southward, as does alongshore wind(Fig. 5a). The model MLD values are realistic as very similar (not shown) to the climatological values (de Boyer Montegut et al., 2004). To contrast the total chlorophyll content with the surface chlorophyll signal, we averaged chlorophyll vertically over the euphotic layer depth and horizontally in the 200 km coastal band and in the 4–15°S latitude range. The variations are portrayed in Fig. 6a, along with those of surface chlorophyll. The depth-averaged chlorophyll shows a similar variability than the surface chlorophyll, albeit with a lower amplitude. The main difference between the two is that the depth-averaged chlorophyll level in early summer (~2.5 mgChl/m^3 in January–February) is rather close to the winter level (~1.5–2 mgChl/m^3 in July–August–September), whereas the summer surface level (~3.5 mgChl/m^3 in January–February) is roughly equal to twice the winter surface level (~1.5–2 mgChl/m^3 in July–August–September). This difference between the surface values and depth-averaged values illustrates the impact of vertical mixing on the vertical profile of chlorophyll, as suggested by Calienes et al. (1985). Note also that the total phytoplanktonic biomass is not well correlated with the variability of upwelling-favorable winds. Fig. 6a displays two distinct peaks in late austral spring (November–December) and late summer (March), whereas the alongshore wind stress is maximum in April and September (Fig. 5a).

Thus, the paradox of low chlorophyll during strong upwelling can be partly explained by the role of vertical mixing. The surface chlorophyll concentration is higher in early summer partly because of surface stratification permits blooms to accumulate. In winter, the upwelling is stronger than in summer (Fig. 6a) but biomass is distributed vertically over a greater MLD, hence the surface chlorophyll concentration is reduced. MLD variations have thus a major impact on the surface chlorophyll seasonal variability and on the vertical distribution of chlorophyll.

To further investigate the role of vertical mixing, two sensitivity experiments were performed with the model. The first experiment

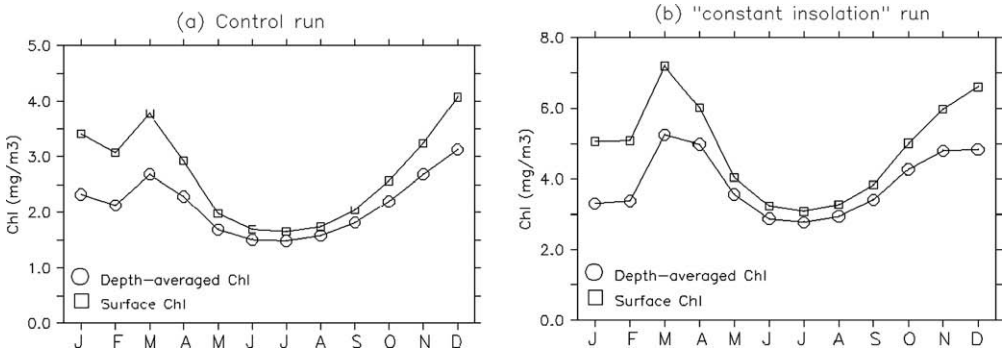

Fig. 6. Time evolution of the ROMS/PISCES surface chlorophyll (squares) and depth-averaged chlorophyll in the euphotic layer (circles) (in mgChl/m^3), horizontally averaged in a 200 km-wide coastal band between 4°S and 15°S: (a) control run; (b) constant insolation run. Note the change of scale between the two figures.

consists in suppressing the seasonality of vertical mixing by imposing a constant MLD and constant vertical mixing coefficients in the biogeochemical part of the model. These model parameters were fixed to annual mean values. In this experiment, the seasonality of the upward nutrient flux is not modified with respect to the control run, and only the mixing coefficients and mixed layer depth used in the biogeochemical tracers equations are kept constant in time. The results of this experiment confirm our hypothesis: with a fixed mixing coefficient and MLD, the seasonality of the surface and depth-averaged chlorophyll is almost totally removed (figure not shown). The signal, averaged over the coastal region defined in Fig. 6, varies between 1.2 and 1.6 mgChl/m^3 throughout the year. This confirms the role of the mixed layer seasonality in driving the seasonality of surface chlorophyll.

Surface temperature may also influence the surface primary productivity through the Q10 effect (Eppley, 1972). Nearshore primary production could reduce in winter because of the surface temperature decrease associated with atmospheric cooling and to the strong wintertime upwelling of cold water. To investigate the impact of this process, we performed an experiment in which the temperature used in the biogeochemical model was kept constant throughout the year, fixed to the annual mean value. As in the previous experiment, the impact of the physics on the ecosystem is unchanged from the control run, except for the temperature effect. The results show a negligible effect (figure not shown). The seasonal variability of surface chlorophyll differs by less than 5% from the control run variability. In conclusion, these two sensitivity experiments show the overwhelming impact of winter vertical mixing on the surface chlorophyll variability at seasonal time scales.

3.4. Nutrient limitation and chlorophyll seasonal variability

Macronutrients such as nitrate, phosphate and silicate were routinely collected during the IMARPE cruises during the 1992–2004 period. The time-latitude evolution of *in situ* and modelled surface nutrients in the 200 km-wide coastal band is shown in Figs. 7 and 8, respectively. Overall, the seasonal cycle of the surface nutrients appears to be in phase by the wind-driven upwelling (Fig. 5a), as high concentrations occur in austral spring and winter. In austral summer, the model macronutrient surface concentrations agree relatively well with the observations, except at latitudes south of 13°S. In winter, the model surface concentrations are higher by a factor of ~2 for nitrate, ~1.5 for silicate and phosphate, than the *in situ* data. This may partly stem from the model biogeochemical tracer initial conditions. PISCES initial and boundary conditions for the macronutrients concentrations were initialized using data from the World Ocean Atlas 2001 (Conkright et al., 2002) data product on a 1° by 1° horizontal grid, which were extrapolated onto the ROMS model 1/6° × 1/6° grid. The model late austral winter (August–September) high nitrate concentrations (~18 μmol/l, Fig. 8a) compare well with WOA data (not shown), but the austral fall and early winter values are much larger than in WOA. A comparison between WOA and IMARPE vertical sections of nitrate shows that the WOA nitrate concentration could be overestimated near the coasts (figure not shown) due to the lack of nearshore profiles in the data base. The high values in the WOA (and hence in the model initial conditions) could be an artefact caused by the extrapolation of offshore high nitrate values towards the coastal margin, where denitrification within the Oxygen Minimum Zone could induce low nitrate concentrations (Wooster et al.,

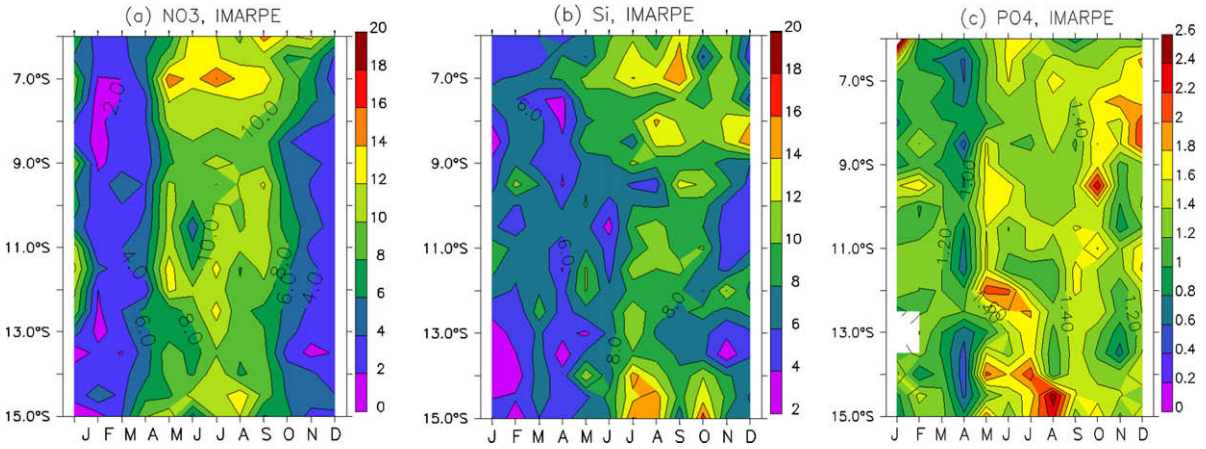

Fig. 7. Time–latitude variations of the surface in situ IMARPE: (a) nitrate; (b) silicate; (c) phosphate surface concentration (in μmol/l) averaged in a 200 km-wide coastal band.

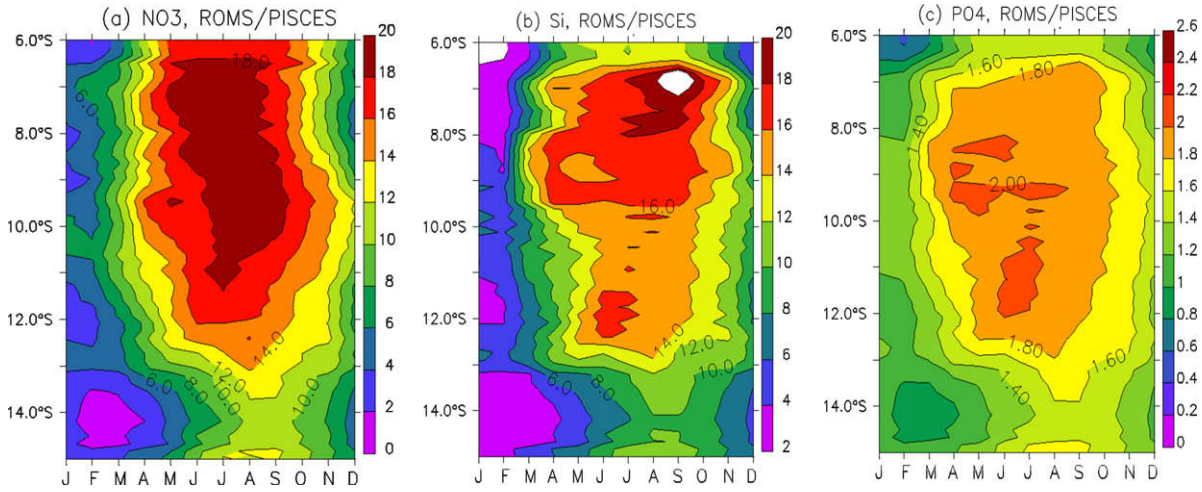

Fig. 8. Same as Fig. 7 for model results.

1965; Ward et al., 1989). On the other hand, the silicate and phosphate concentrations compare well with WOA and IMARPE data (not shown), and the model winter values remain higher than the observations (Figs. 7b–c and 8b–c). This suggests that the austral winter upwelling of nutrients may be too strong in the model, consistent with the higher than observed model surface chlorophyll values (Figs. 3 and 4).

Nutrient and light limitation of the primary production can be quantified by computing explicitly the limitation terms in the primary production model parameterizations. The model primary production is proportional to the product of a light limitation term and a nutrient limitation term. The nutrient limitation term L_{nut} is the minimum of a set of (n) Michaelis–Menten nutrients limitation factors, namely $L_{\mathrm{nut}} = \min_{i=1,\ldots,n}[C_i/(K_i + C_i)]$ where the index (i) denotes a specific nutrient, C_i its concentration and K_i its half-saturation constant. The light limitation term L_{light} is equal to $[1 - \exp(-\alpha\,(\mathrm{Chl/C}) \cdot \mathrm{PAR}/(\mu \mathrm{Lnut})]$ where α is the initial slope of the PI curve, Chl/C the chlorophyll over carbon ratio, PAR the photosynthetically available radiation, μ the growth rate depending on temperature. When enough light is available this term saturates to 1, whereas it remains less than 1 when light limits the growth. We chose to focus on the limitation terms of diatom growth, as they contribute to more than 70% of the total chlorophyll concentration in the region.

The cross-shore vertical structure of the limiting nutrient is portrayed for different time periods in Fig. 9. In the well-lit, shallow mixed layer which establishes during austral summer, diatom growth is limited by nitrate within ~100 km from the coast, and then by silicate further offshore (Fig. 9a–b). Because of the relatively weak upwelling and offshore Ekman transport during summer, phytoplankton growth is constrained by the upward flux of macronutrients such as nitrate and silicate, which are consumed rapidly after they reach the surface. Fe availability limits the growth in a thin subsurface layer located offshore. The nearshore Fe concentration is relatively high since it is supplied by the continental shelf sediments. Due to offshore Ekman transport and shallow mixed layer during summertime, Fe is advected offshore and remains confined near the surface, hence limiting phytoplankton growth below the mixed layer. Note that light limitation occurs at very shallow depths (~2–4 m) nearshore and at greater depths (~10 m) 100 km from the shore (Fig. 9a and 9b) because of the high chlorophyll concentration in the surface layer near the coast.

During austral winter, the limiting factors change drastically (Fig. 9c). Silicate is brought to the surface by the strong coastal upwelling and advected offshore by Ekman currents, thus is no longer limiting offshore as during summertime. At ~100 km from the shore, nutrient limitation shifts to Fe. Note that because of the increased wintertime vertical mixing, Fe is diluted vertically. Its concentration decreases and remains sufficiently high to avoid Fe limitation only within ~100 km from the coast. In the vertical, light availability is the dominant limiting factor over most of the mixed layer.

To further investigate the impact of Fe limitation on phytoplankton growth, it was artificially turned off in the PISCES model in order to evaluate its impact on the ecosystem. This induced a surface chlorophyll increase by ~20–40% north of 9°S during most of the year (Fig. 10). The increase reached ~40–50% in austral spring between 9°S and 11°S. The impact was strongest near 14°S, where the productivity resulted in a two-fold biomass increase, reaching realistic levels of ~1.5–2 mgChl/m^3. However, the late spring–summer model bias was not significantly reduced, suggesting that Fe limitation may not be the only issue near 14°S. In conclusion, this sensitivity experiment confirms that Fe is the main limiting nutrient off the shelf in winter in our model, and that the productivity can be increased when Fe limitation is relaxed. In contrast, nutrient limitation shifts to macronutrients such as nitrate and phosphate during summer. Fe limitation of diatom blooms off the Peruvian shelf has been observed during the late austral winter of 2000 (Hutchins et al., 2002; Bruland et al., 2004; Hare et al., 2005) and these observations support our hypothesis. However, note that the modelled biomass increase due to the relaxation of Fe limitation near 8°S remains moderate (~20–40%, Fig. 10). This suggests that light limitation due to the winter MLD increase or to the lower winter insolation, is the main factor controlling the winter productivity. This will be investigated in more detail in the next section. Moreover, Fe and light conditions are closely related as Fe limitation may be enhanced by the higher Fe requirement of phytoplankton cells when light conditions are less favourable (e.g., Sunda and Huntsman, 1997).

3.5. Light limitation and the seasonal variability of chlorophyll

Insolation displays significant seasonal variations over the Peru area. On average, the COADS climatological nearshore solar flux is maximum in austral summer (between 240 and 280 W/m^2) and minimum in austral winter (between 120 and 160 W/m^2). The amplitude of the insolation cycle is maximum near 15°S (figure not shown). We now investigate the impact of these variations on surface chlorophyll. In a sensitivity experiment, the seasonal variations of insolation were suppressed in the biological model.

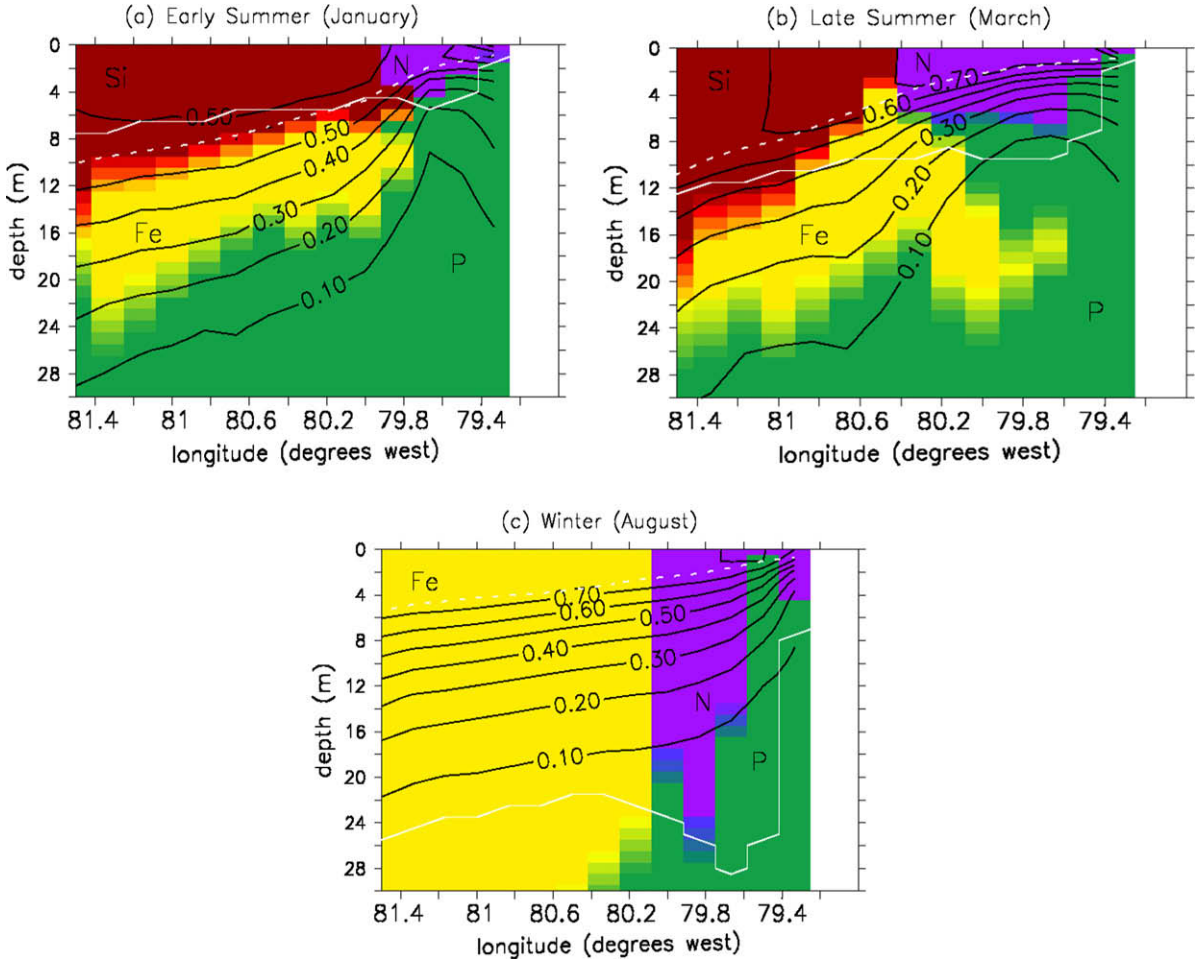

Fig. 9. Diatoms colimitations at 8°S: (a) early summer (January); (b) late summer (March); (c) winter (July). Colors and labels indicate the limiting nutrient (purple: nitrate (N), yellow: iron (Fe), green: phosphate (P), red: silicate (Si)). The dashed white line indicates the depth at which the limitation shifts from nutrients (above the line) to light (below the line). Labeled black contours indicate the value of the light limiting coefficient (L). The full white line indicates the mixed layer depth.

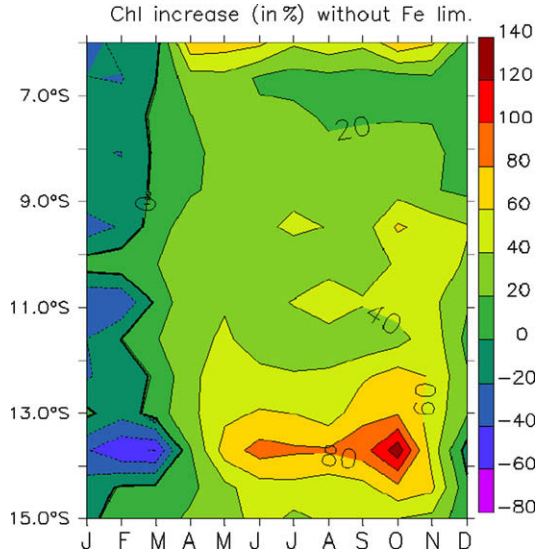

Fig. 10. Time–latitude evolution of the surface chlorophyll increase (in%) when Fe limitation is relaxed in the ROMS/PISCES model.

The heat fluxes (including the heating effect of the short wave solar radiations) vary seasonally in ROMS physical and thermodynamical components, in order to keep the MLD, vertical mixing and thermal stratification unchanged with respect to the control run. In contrast, the solar radiation available for phytoplankton growth is kept constant with time and latitude throughout the simulation. It is fixed to 190 W/m^2, which corresponds to the year-averaged value over a 200-km-wide band of coastal ocean band between 6°S and 15°S.

The average chlorophyll seasonal cycle is represented in Fig. 6b. First, note that the mean level of surface chlorophyll (~4–5 mgCh/m^3) is greater than in the control run (~2.5–3 mgCh/m^3, Fig. 6a). This rather surprising result can be explained by the significant light limitation of winter productivity in the control run. A 25% increase in solar radiation during winter (190 W/m^2 instead of 150 W/m^2) in the "light-pertubed" simulation generates a two-fold increase in depth-averaged biomass during winter (Fig. 6). This accumulated biomass produces a significant pool of ammonium in the subsurface layers (figure not shown), which is consumed during the spring and fall bloom. This effect is substantial as biomass doubles during summer in the "light-perturbed" simulation in spite of a light level lower (by ~30%) than in the control run. The important result of this experiment is that the characteristics of the surface chlorophyll seasonal variations are unchanged (Fig. 6b) with respect to the control run (Fig. 6a). The seasonality remains both in the surface and depth-averaged chlorophyll signals. This indicates that the total phytoplankton biomass varies regardless of the insolation cycle, because of spring restratification and fall destratification induced by vertical mixing, as in open-

ocean oligotrophic regions. The effect of vertical mixing can be estimated by comparing the summer and winter depth-averaged biomass in Fig. 6b. They are relatively close (~3.5 and ~2.5 mgCh/m^3, respectively) during the two periods, whereas the surface values differ by ~2–2.5 mgChl/m^3. The sudden rise in depth-averaged biomass of about 1.5 mgChl/m^3 between February and March results from an MLD increase which entrains regenerated nutrients (NH_4) into the shallow, well-lit surface layer, and generates a fall bloom.

To conclude, the model experiments show that the insolation seasonal variations have a weak impact on the seasonal cycle of surface chlorophyll, and that vertical mixing acts in two different ways. Firstly, phytoplankton is distributed over a greater depth in winter than in summer. Hence, the winter surface chlorophyll concentration decrease is caused by a purely physical vertical dilution and by a primary production decrease due to light limitation. Light limitation is mainly caused by the MLD increase, and not by the reduced insolation during winter. The decrease in vertical mixing in late winter-spring induces a restratification phase, during which light limitation is relaxed, allowing phytoplankton to grow until the surface regenerated nutrients are consumed. Secondly, in austral fall, the mixed layer depth increases and entrains new nutrients into the mixed layer, which generates the March bloom.

4. Discussion

Satellite data, *in situ* observations and model results display a surface chlorophyll seasonal variability near the Peruvain coasts which is in phase opposition with the dynamical forcing of the coastal upwelling. The observed variability has been well reproduced with the ROMS/PISCES coupled model, especially off northern Peru (6–10°S). Further south, the simulated amplitude of the seasonal cycle is reduced compared to observations.

Several hypotheses may explain the model's lack of realism south of 10°S. The first one is the morphology of the continental shelf in the model, which could have an impact on the input of Fe from the sediments. A wider continental shelf implies a larger Fe supply from the sediments. As a consequence, the upwelled waters north of 10°S contain more Fe because the shelf is widest there (Bruland et al., 2004). In the ROMS model, bottom topography has been smoothed in order to reduce the slope near the shelf break and verify numerical criteria which limit error on the horizontal pressure gradient (Mellor et al., 1998). Because of this smoothing procedure, the shelf off Peru is narrower in the model than in reality, especially south of 11°S. Since Fe appears to be the limiting nutrient during winter, this model artifact could limit excessively the development of phytoplanktonic biomass south of 10°S.

The absence of intraseasonal variability in the physical forcing of the model (the atmospheric forcing and the model's open boundary conditions (hereafter OBCs)) may also impact chlorophyll variability. Indeed, the OBCs of the model are seasonal and cyclic. In the Equatorial Pacific, the intraseasonal eastward propagating equatorial Kelvin waves, which trigger poleward propagating coastally trapped waves when reaching the American coast, have been filtered from the OBC. These coastal waves may shoal or depress the nutricline along the coast, and generate westward-propagating Rossby waves which advect surface chlorophyll offshore (Bonhomme et al., 2007).

Coastal waves may impact nearshore biological productivity, whereas Rossby waves may extend the biologically productive coastal zone further offshore. To investigate the potential impact of this variability on the seasonal cycle, model experiments should be performed with the full spectrum of variability at the OBCs. Let us now focus on the nutrients issue. On the one hand, the surface and subsurface (not shown) macronutrient (nitrate, silicate and phosphate) concentrations are higher in the model simulation than in the IMARPE *in situ* data (Figs. 7 and 8). On the other hand, the model outputs are consistent with the very high values of NO_3 from the WOA data base, which were used to initialize the model. To explain these differences between the WOA data base and the IMARPE measurements, a dedicated study of the WOA and IMARPE nitrate profiles should be conducted in the future. Furthermore, the physical model may be partly responsible for the nutrient bias. Indeed, the seasonal cycle of the polewards-flowing Peru/Chile Undercurrent, which transports most of the water mass upwelled near the coast, is not well known and may not be very well represented in the model. A vertical section of WOA density in July near 8°S (not shown) shows that the subsurface isopycnals and nitrate isolines tend to deepen toward the coast. This suggests an increase in the PCUC transport which is not reproduced by the model. The question of the impact of the circulation on macronutrient supply remains open and should be addressed in future work.

5. Conclusions

The seasonal variability of the surface chlorophyll concentration in the Peru upwelling system were studied using *in situ* observations, satellite data and results from a three dimensional regional model coupling ocean dynamics (ROMS) and biogeochemical cycles (PISCES). The SeaWiFS satellite data and IMARPE *in situ* observations display a strong seasonality with low values in austral winter and high values in austral spring and summer, in phase opposition to upwelling intensity (Bakun and Nelson, 1991). The modelled surface chlorophyll seasonal cycle is similar in pattern and values are in general between the IMARPE and SeaWIFS data.

The mechanisms controlling the chlorophyll seasonality were investigated using model experiments. The deepening of the mixed layer was shown to be mainly responsible for the decrease of surface chlorophyll in austral winter, confirming previous observational studies (Calienes et al., 1985). The phytoplanktonic biomass increased significantly in austral spring and fall following periods of restratification and destratification, respectively. The PCU system is almost as productive in austral winter as in early summer, and the decrease in surface biomass in winter results from a dilution and light limitation effect, and that the reduced insolation during winter does not affect the amplitude and phase of the surface chlorophyll signal.

Nutrient limitations of phytoplankton growth were studied in the model. Fe appears to be the limiting nutrient off northern Peru during winter in the model, which is consistent with several recent studies based on *in situ* Fe measurements (Hutchins et al., 2002; Bruland et al., 2004). In summer, the upwelling is weaker and the model limitation shifts to macronutrients such as nitrate and silicate. Future studies will investigate the impact of dynamical processes at higher resolution and of an improved atmospheric forcing on the surface productivity, and will address the intraseasonal and interannual variability in the Peru upwelling.

Acknowledgements

Model simulations were performed on NEC-SX5 and NEC-SX8 IDRIS (Institut du Développement et de Ressources en Informatique Scientifique) computers. J. Ledesma was financially supported by the DSF (Département Soutien et Formation) of IRD (Institut de Recherche pour le Développement). The collaborative work between IRD and IMARPE was sponsored by the IRD ATI "Sistema de Humboldt". We also thank Cyril Lathuilière from LOCEAN for extracting and processing SeaWiFS data.

Appendix A

A.1. IMARPE chlorophyll-*a* measurements

The chlorophyll measurements are made using the standard fluorometric procedure of Holm-Hansen et al. (1965). Chlorophyll-*a* pigments are retained by micro-filters (Whatman GF/F 0.75 μm). The 100 ml sea water samples are then freezed for further analysis. The pigments are extracted in acetone for periods of 3 h. Chlorophyll is then calculated from results obtained with a Turner Design (AU-10 Model) previously calibrated with commercial Chl-*a* from (Sigma Chemical Co.) This method is adapted for a range of measurements between 0.01 and 200.00 mg/m^3, with a precision of ±0.20 mg/m^3. Quality control consisted in computing a climatology in 0.5° × 0.5° bins, comparing each of the chlorophyll values to the climatology, and filtering the extreme values.

A.2. IMARPE nutrient measurements

The water samples were collected and freezed on board for later measurements. Nutrients were measured following the spectrophotometric method described in Strickland and Parson (1972) using a Perkin–Elmer Lambda 40 double-beam UV/Vis spectrophotometer.

References

Aumont, O., Bopp, L., 2006. Globalizing results from ocean *in situ* iron fertilization studies. Global Biogeochemical Cycles 20 (2). doi:10.1029/2005GB00259.

Aumont, O., Maier-Reimer, E., Blain, S., Monfray, P., 2003. An ecosystem model of the global ocean including Fe, Si, P colimitations. Global Biogeochemical Cycles 17 (2), 1060.

Bakun, A., Nelson, C.S., 1991. The seasonal cycle of wind stress curl in sub-tropical boundary current regions. Journal of Physical Oceanography 21, 1815–1834.

Bonhomme, C., Aumont, O., Echevin, V., 2007. Advective transport caused by intraseasonal Rossby waves: a key player of the high chlorophyll variability off the Peru upwelling region. Journal of Geophysical Research 112, C09018. doi:10.1029/2006JC004022.

Bruland, K.W., Rue, E.L., Smith, G.J., DiTullio, G.R., 2004. Iron, macronutrients and diatom blooms in the Peru Upwelling regime: brown and blue waters of Peru. Marine Chemistry 93, 81–103.

De Boyer Montégut, C., Madec, G., Fisher, A.S., Lazar, A., Iudicone, D., 2004. Mixed layer depth over the global ocean: an examination of profile data and a profile-based climatology. Journal of Geophysical Research 109, C12003. doi:10.1029/2004JC002378.

Calienes, R., Guillen, O., Lostanau, N., 1985. Variabilidad espacio temporal de clorofila, produccion primaria y nutrients frente a la costa peruana. IMARPE bolletin, Callao. 44.

Carr, M.-E., Strub, P.T., Thomas, A.C., Blanco, J.L., 2002. Evolution of 1996–1999 La Nina and El Nino conditions off the western coast of South America: a remote sensing perspective. Journal of Geophysical Research 107 (12), 3236. doi:10.1029/2001JC001183.

Chavez, F.P., 1995. A comparison of ship and satellite chlorophyll from California and Peru. Journal of Geophysical Research 100 (C12), 24855–24862.

Chavez, F.P., Ryan, J., Lluch-Cota, S.E., Niquen, M., 2003. From anchovies to sardines and back: multidecadal change in the Pacific ocean. Nature 299, 217–221.

Conkright, M.E., Locarnini, R.A., Garcia, H. E., O'Brien, T.D., Boyer, T.P., Stephens, C. Antononov, J. (2002). World Ocean Atlas 2001: objectives, analyses, data statistics and figures [CD-ROM], NOAA Atlas NESDIS 42, Silver Spring, Md.

Croquette, M., Eldin, G., Grados, C., Tamayo, M., 2007. On differences in satellite wind products and their effects in estimating coastal upwelling processes in the south-east Pacific. Geophysical Research Letters 34, L11608. doi:10.1029/2006GL027538.

Da Silva, A.M., Young, C.C., Levitus, S., 1994. Atlas of surface marina data 1994, vol. 1, Algorithms and procedures, technical report, Natl. Oceanogr. And Atmos. Admin., Silver Spring, Md.

DiTullio, G., Geesey, M.E., Maucher, J.M., Alm, M.B., Riseman, S.F., Bruland, K.W., 2005. Influence of iron on algal community composition and physiological status in the Peru upwelling system. Limnology Oceanography 50, 1887–1987.

Eppley, R.W., 1972. Temperature and phytoplankton growth in the sea. Fishery Bulletin, 1063–1085.

FAO (Food Administration Organisation), (1999). The state of world fisheries and aquaculture 1998. FAO Documentation Group, Rome, Italy.

Gorgues, T., Menkes, C., Aumont, O., Vialard, J., Dandonneau, Y., Bopp, L., 2005. Biogeochemical impact of tropical instability waves in the Equatorial Pacific. Geophysical Research Letters 32, L24615. doi:10.1029/2005GL024110.

Gruber, N., Frenzel, H., Doney, S.C., Marchesiello, P., McWilliams, J.C., Moisan, J.R., Oram, J.J., Plattner, G.K., Stolzenbach, K.D., 2006. Eddy-resolving simulation of plankton ecosystem dynamics in the California Current System. Deep Sea Research I 53, 1483–1516.

Guillen, O., Calienes, R., 1981. Upwelling off Chimbote. Coastal and Estuarine Science 1, 312–326.

Hare, C.E., DiTullio, G.R., Trick, C.G., Wilhelm, S., Bruland, K.W., Rue, E.L., Hutchins, D.A., 2005. Phytoplankton community structure changes following simulated upwelled iron inputs in the Peru Upwelling region. Aquatic Microbial Ecology 38, 269–282.

Holm-Hansen, O., Lorenzen, C.J., Holmes, R.W., Strickland, J.D.H., 1965. Fluorometric determination of chlorophyll. Journal du Conseil Permanent International pour L'Exploration de la Mer 30 (1), 3–15.

Hooker, S.B., McClain, C.R., 2000. The calibration and validation of SeaWiFS data. Progress in Oceanography 45, 427–465.

Hutchins, D.A., Hare, C.E., Weaver, R.S., Zhang, Y., Firme, G.F., DiTullio, G.R., Alm, M.B., Riseman, S.F., Maucher, J.M., Geesey, M.E., Trick, C.G., Smith, G.J., Rue, E.L., Conn, J., Bruland, K.W., 2002. Phytoplankton iron limitation in the Humboldt Current and Peru Upwelling. Limnology and Oceanography 47, 997–1011.

Iriartre, J.L., Gonzalez, H.E., 2004. Phytoplankton size structure during and after the 1997/1998 El Nino in coastal upwelling area of the northern Humboldt Current System. Marine Ecology Progress Series 269, 83–90.

Large, W.G., McWilliams, J.C., Doney, S.C., 1994. Oceanic vertical mixing: a review and a model with a nonlocal boundary layer parameterization. Review of Geophysics 32, 363–403.

Madec, G., Delecluse, P., Imbard, M., Lévy, C., 1998. OPA 8.1, ocean general circulation model reference manual. *Notes du pôle de Modélisation, 11*, Institut Pierre-Simon Laplace (IPSL).

Mellor, G.L., Oey, L.-Y., Ezer, T., 1998. Sigma coordinate pressure gradient errors and the seamount problem. Journal of Atmospheric and Oceanic Technology 15 (5), 1122–1131.

Minas, H.J., Coste, B., Minas, M., Raimbault, P., 1990. Conditions hydrologiques, chimiques et production primaire dans les upwellings du Pérou et des îles Galapagos, en régime d'hiver austral (campagne Paciprod). Oceanologica Acta (10), 383–391.

Pennington, J.T., Mahoney, K.L., Kuwahara, V.S., Kober, D.D., Calienes, R., Chavez, F.P., 2006. Primary production in the eastern tropical pacific: a review. Progress in Oceanography 69 (2–4), 285–317.

Paulmier, A., Ruiz-Pino, D., Garçon, V., Farias, L., 2006. Maintaining of the Eastern South Pacific Oxygen Minimum Zone (OMZ) off Chile. Geophysical Research Letters 33, L20601. doi:10.1029/2006GL026801.

Penven, P., Echevin, V., Pasapera, J., Colas, F., Tam, J., 2005. Average circulation, seasonal cycle, and mesoscale dynamics of the Peru Current System: a modeling approach. Journal of Geophysical Research 110 (C10), C10021. doi:10.1029/2005JC002945.

Shchepetkin, A.F., McWilliams, J.C., 2005. The regional oceanic modeling system: a split-explicit, free-surface, topography-following-coordinate ocean model. Ocean Modelling (9), 347–404.

Strickland, J., Parson, T., 1972. Practical Handbook of Seawater Analysis. Fisheries Board of Canada Ottawa, Bulletin. 167.

Strub, P.T., Mesías, J.M., Montecino, V., Rutllant, J., 1998. Coastal ocean circulation off western South America. In: Robinson, A.R., Brink, K.H. (Eds.), The Global Coastal Ocean. The Sea, 11, Interscience, New York, pp. 273–313.

Sunda, W.G., Huntsman, S.A., 1997. Interrelated influence of iron, light and cell size on marine phytoplankton growth. Nature 390, 389–392.

Tegen, I., Fung, I., 1995. Contribution to the atmospheric mineral aerosol load from land surface modification. Journal of Geophysical Research 100, 18707–18726.

Thomas, A.C., Carr, M.E., Strub, P.T., 2001. Chlorophyll variability in eastern boundary currents. Geophysical Research Letters 28 (18), 3421–3424.

Ulloa, O., Escribano, R., Hormazabal, S., Quinones, R.A., Gonzalez, R.R., Ramos, M., 2001. Evolution and biological effects of the 1997–1998 El Nino in the upwelling ecosystem off northern Chile. Geophysical Research Letters 28 (8), 1591–1594.

Ward, B.B., Glover, H.E., Lipschultz, F., 1989. Chemoautotrophic activity and nitrification in the oxygen minimum zone off Peru. Deep Sea Research 36, 1031–1051.

Wooster, W.S., Chow, T.J., Barret, I., 1965. Nitrite distribution in the Peru current waters. Journal of Marine Research 23, 210–221.

Wyrtki, K., 1962. The oxygen minima in relation to ocean circulation. Deep Sea Research 9, 11.